

Near-infrared imaging of 222 nearby H δ -strong galaxies from the SDSS¹

Michael L. Balogh^{2,3}, Chris Miller⁴, Robert Nichol⁵, Ann Zabludoff⁶ & Tomo Goto⁷

¹Based on observations made with the United Kingdom Infrared Telescope

²Department of Physics, University of Waterloo, Waterloo, ON, Canada N2L 3G1

³E-mail: mbalogh@uwaterloo.ca

⁴Cerro-Tololo Inter-American Observatory, NOAO, Casilla 603, La Serena, Chile

⁵Institute of Cosmology and Gravitation, Mercantile House, Hampshire Terrace, University of Portsmouth, Portsmouth, UK PO1 2EG

⁶Steward Observatory, University of Arizona Tucson, AZ, 85721 USA

⁷Space Telescope Science Institute, 3700 San Martin, Baltimore, MD 21218

2 February 2008

ABSTRACT

We present UFTI K-band imaging observations of 222 galaxies that are selected from the Sloan Digital Sky Survey to have unusually strong H δ absorption equivalent widths, $W_{\circ}(\text{H}\delta) > 4\text{\AA}$. Using GIM2D, the images are fit with two-dimensional surface brightness models consisting of a simple disk and bulge component to derive the fraction of luminosity in the bulge, B/T . We find that the galaxies with weak or absent H α or [OII] $\lambda 3727$ emission (known as k+a galaxies) are predominantly bulge-dominated (with a mode of $B/T \sim 0.6$), while galaxies with nebular emission (known as e[a] galaxies) are mostly disk-dominated ($B/T \sim 0.1$). The morphologies and $(r - k)$ colours of most k+a galaxies are inconsistent with the hypothesis that they result from the truncation of star formation in normal, spiral galaxies. However, their $(u - g)$ and $(r - k)$ colours, as well as their H δ line strengths, form a sequence that is well matched by a model in which > 5 per cent of the stellar mass has been produced in a recent starburst. The lack of scatter in the dust-sensitive $(r - k)$ colours suggests that the unusual spectra of k+a galaxies are not due to the effects of dust. The e(a) galaxies, on the other hand, have a colour distribution that is distinct from the k+a population, and typical of normal or dusty ($\tau_V \sim 2$) spiral galaxies. We conclude that many e(a) galaxies are not progenitors of k+a galaxies, but are a separate phenomenon. Both k+a and e(a) galaxies reside in environments (characterized by the local density of galaxies brighter than $M_r = -20$) that are typical of normal galaxies and that are inconsistent with overdense regions like rich galaxy clusters.

Key words: galaxies: evolution — galaxies: interactions — galaxies: structure — galaxies: absorption lines — infrared: galaxies

1 INTRODUCTION

A possible interpretation of the diverse properties of galaxies is that, under the right circumstances, they can transform from one type to another (e.g. Baldry et al. 2004). For example, galaxy mergers are an effective way to transform gas-rich, star-forming spiral galaxies into gas-poor, passively evolving elliptical galaxies (Barnes 1992; Springel 2000). Support for this interpretation is best obtained by finding examples of galaxies in the process of transformation; however, these examples will be rare if the transformation timescale is short.

One of the best candidates for such a transition population is the class of galaxies with spectra that have unusually strong Balmer-line absorption, but that lack emission lines. Although originally discovered in galaxy clusters at $z \sim 0.3$

(Dressler & Gunn 1982), later work showed that these galaxies are also found in low-density environments, at low redshift (Zabludoff et al. 1996; Castander et al. 2001; Goto et al. 2003; Quintero et al. 2004) and at higher redshift (Dressler et al. 1999; Balogh et al. 1999). Stellar population synthesis modelling suggests that the spectra are best modelled as a post-starburst, with all star formation ceasing following the burst (Couch & Sharples 1987; Dressler & Gunn 1992; Barger et al. 1996; Poggianti et al. 1999; Balogh et al. 1999). Less extreme examples (i.e. with weaker Balmer absorption lines) do not necessarily require a burst, but can be modelled as a normal star-forming galaxy in which star formation is suddenly truncated. Since the lifetime of the enhanced Balmer lines is short ($\lesssim 0.5$ Gyr), even a small observed population of such galaxies might indicate that a significant fraction of

all galaxies have undergone a transformation via this phase; it is even possible that they represent the route by which all early-type galaxies form (Norton et al. 2001; Tran et al. 2003).

The spectral properties (e.g. line strengths) of these unusual galaxies are not completely disjoint from those of the normal galaxy population, but rather represent the tail of a continuous distribution (e.g. Zabludoff et al. 1996; Balogh et al. 1999). Given the large number of free parameters available to model the spectra (e.g. metallicity, initial mass function, and multi-component dust models, in addition to the parametrization of the star formation history), it is not therefore possible to uniquely define the spectral characteristics of a post-starburst galaxy, and this has led to a variety of definitions and nomenclatures. We will adopt the nomenclature (but not the precise definition) of Dressler et al. (1999), and call galaxies with strong Balmer absorption, but no detectable nebular emission, k+a galaxies (because the spectrum approximately resembles a combination of k-star and a-star spectra). Galaxies with strong Balmer lines and some emission we will refer to as e(a). Furthermore, for clarity, when referring to previous work we will retain this nomenclature, although the definitions vary significantly between samples. In particular, the use of the H α emission line, often not available in earlier spectroscopic samples, makes a significant difference to the sample selection (e.g. Abraham et al. 1996; Quintero et al. 2004; Blake et al. 2004). Our precise definitions of the k+a and e(a) galaxies are given in § 2.1.

The spectra of e(a) galaxies are even more difficult to interpret than those of k+a galaxies, as it is difficult to find a model that predicts both emission lines (arising from star formation rather than an active nucleus) and strong Balmer absorption. This is primarily because the OB stars, which dominate the optical luminosity and are required to produce the emission lines, have intrinsically weak Balmer absorption lines. Thus, the relationship between k+a and e(a) galaxies is unknown. One possible model is that e(a) galaxies have a two-phase dust distribution, in which the OB stars are preferentially obscured, relative to the A-stars (Poggianti & Wu 2000). It has been suggested (Poggianti et al. 1999) that some e(a) galaxies may be in the midst of a dust-obscured starburst and will resemble k+a galaxies when the star formation ends. The fact that some merging starburst systems and ultraluminous infrared galaxies exhibit e(a) spectra may support this hypothesis (Liu & Kennicutt 1995). Another possibility is that some k+a galaxies are extreme examples of the e(a) phenomenon, where the dust obscuration is strong enough to completely eliminate the emission lines (Smail et al. 1999; Balogh & Morris 2000). However, this latter interpretation is not likely the case for the majority of the k+a population, which are undetected in HI and radio continuum (Chang et al. 2001; Miller & Owen 2001).

Until recently, detailed studies of k+a and e(a) galaxies have been limited to small samples (e.g. Zabludoff et al. 1996; Galaz 2000). Long-slit spectroscopy (Norton et al. 2001) and high-resolution *Hubble Space Telescope* imaging (Yang et al. 2004) of some k+a galaxies suggest that they result from the recent merger of gas-rich disk galaxies and will evolve into relaxed spheroidal galaxies that lie on the fundamental plane. However, because of the small sample size it is not clear how general the interpretation is (e.g. Galaz 2000; Caldwell et al. 1996; Bartholomew et al. 2001; Tran et al. 2003). Recently, large samples of nearby k+a and e(a) galaxies have been compiled from the Sloan Digital Sky Survey (Goto et al. 2003; Quintero et al. 2004) and the 2dF Galaxy Redshift Survey (Blake et al. 2004). These studies confirm the extreme rarity of such galaxies; for example, Goto et al. (2003) find that < 0.1 per cent of all galaxies satisfy our definition of a k+a

galaxy. Quintero et al. (2004) and Blake et al. (2004) find that most of these galaxies are bulge-dominated and are found in all environments. However, the morphologies are based on visual light, which is sensitive to recent star formation. In the present paper, we present near-infrared observations for a large sample of k+a and e(a) galaxies drawn from the Goto et al. (2003) sample to directly study the stellar mass and its morphological distribution.

The paper is structured as follows. In § 2 we describe the galaxy sample and the photometric and morphological measurements. The main results are presented in § 3, and the colours, H δ line strengths and luminosities are compared with various model predictions in § 4. Our conclusions regarding the connection between e(a) and k+a galaxies, as well as a comparison with other results in the literature, are given in § 5. Finally we summarize our findings in § 6. For cosmology-dependent quantities, we assume a matter density $\Omega_m = 0.3$, a dark energy component $\Omega_\Lambda = 0.7$ and a Hubble constant of $70 \text{ km s}^{-1} \text{ Mpc}^{-1}$.

2 DATA

2.1 The Galaxy Sample

We selected our sample from the catalogue of Goto et al. (2003), based on the first data release of the Sloan Digital Sky Survey (Abazajian et al. 2003). This catalogue contains all galaxies for which the rest frame equivalent width of the H δ absorption line is $W_\circ(\text{H}\delta) > 4\text{\AA}$ (with 2σ confidence), as measured from the spectrum using a Gaussian-fitting technique. A second Gaussian was fit to correct for emission-filling when emission lines are present. From this sample, we identify two main types of galaxies: e(a) galaxies have either H α or [OII] detected in emission with at least 2σ confidence (but see below), while for k+a galaxies these emission lines are undetected at the same significance level. These definitions are similar in spirit to those of Dressler et al. (1999). However, our definition of a k+a galaxy is stricter in the sense that we require both stronger absorption in H δ (4\AA compared with 3\AA) and our data quality and wavelength coverage allows us to be more comprehensive in excluding galaxies with emission lines (Dressler et al. 1999, require only that $W_\circ([\text{OII}]) < 5\text{\AA}$). In particular, H α is a more sensitive indicator of star formation than [OII], and its inclusion in the selection criteria is important (e.g. Abraham et al. 1996; Quintero et al. 2004; Blake et al. 2004). However, in this work we will show that the properties of e(a) galaxies with only weak emission lines, $W_\circ(\text{H}\alpha) < 10\text{\AA}$ and $W_\circ([\text{OII}]) < 10\text{\AA}$, are similar to k+a galaxies (i.e. those without any emission). We will therefore find it convenient to exclude these from the e(a) sample, and present them as a third class of galaxy. Not wishing to complicate the nomenclature further, we will simply refer to them as k+a galaxies with weak emission.

From this catalogue, we selected galaxies with $z > 0.05$ and surface brightness $z' < 21.25 \text{ mag arcsec}^{-2}$ for infrared observations. The selection was mostly random, though preference was given to k+a galaxies over the more common e(a) galaxies. Furthermore, we excluded a few galaxies that showed emission line ratios clearly indicative of an active nucleus. For weak emission lines, the strong underlying absorption that is characteristic of e(a) galaxies makes it difficult to measure robust line ratios and, therefore, we cannot exclude the possibility that some of these galaxies have a contribution to their emission from an active nucleus. The target list of 128 k+a galaxies (including those with weak emission) is given in Table 1. This gives the positions (columns 1 and 2), redshift (column 3) and r magnitude (column 4) from the SDSS catalogue. The

remaining columns list derived quantities that are described later in the paper, as appropriate. Table 2 lists the same quantities for the 94 e(a) galaxies in the sample. This is smaller than the k+a sample because we preferentially observed k+a galaxies; in a magnitude-limited sample, e(a) galaxies are at least twice as common as k+a galaxies (Goto et al. 2003).

As a comparison sample, we take galaxies from the second data release of the SDSS (Abazajian et al. 2004); 99756 of these have infrared magnitudes that are available from the 2MASS (Jarrett et al. 2000) catalogue, which is complete to $K_s = 13.9$. In particular, we will use the u , g , and r magnitudes from the SDSS catalogue. The $(u - g)$ colour is particularly important as it has been shown to effectively divide galaxies into two distinct populations, based on their star formation rate (e.g. Strateva et al. 2001; Baldry et al. 2004). These data will be compared with our k+a and e(a) galaxy samples in relatively small redshift bins, so differences in the overall redshift distribution are not important.

2.2 Near infrared Observations

Observations were made with the UFTI near-infrared imaging spectrograph on UKIRT over two semesters. In semester 02B we observed in classical mode over Aug 23-30. Weather conditions were mixed, but we obtained H and K-band images of 144 galaxies in 4 clear nights. In semester 03A we were awarded an additional 33 hours of queue-scheduled observing time to complete the observations, and another 100 galaxies were imaged in good conditions over that semester.

The K -band integrations were 600s long, dithered in a 9-point pattern. The exposures in H were shorter (75s), and dithered in a 5-point pattern. Dark frames were obtained 2–3 times per night. Data reduction was performed using the standard UKIRT pipeline reduction tool, which aligns the dithered images and subtracts a sky frame made from the data.

2.3 Measurements

2.3.1 Photometry

Photometry was performed with the IRAF task *qphot* by computing the flux within a circular aperture and subtracting the sky flux measured in an annulus outside this aperture. To provide the best match with the SDSS photometry, we compute the flux within an aperture that is twice as large as the R-band Petrosian radius. This magnitude, corrected for Galactic extinction using the dust maps of Schlegel et al. (1998), is then directly comparable to the magnitudes used to compute Petrosian colours in the optical SDSS bands.

Standard stars were observed throughout both runs to calibrate the photometry; however, non-photometric conditions, particularly during the classically-scheduled first run, mean this calibration is unreliable. To establish the zeropoint with better precision, we compare the aperture photometry within a $5''$ aperture with the equivalent aperture photometry from the 2MASS, where available. Using this comparison, we trace zeropoint changes as a function of time through each run, and this way are able to calibrate the data to within ~ 0.08 mag; this zeropoint uncertainty always dominates our statistical uncertainty. All our observations were made near zenith and no airmass corrections were applied. We do not correct our magnitudes for Galactic extinction, as this correction is typically $\lesssim 0.01$ mag in the K -band.

In Figure 1 we show the distribution of the difference between our total (Petrosian) magnitudes and the Kron elliptical magnitudes

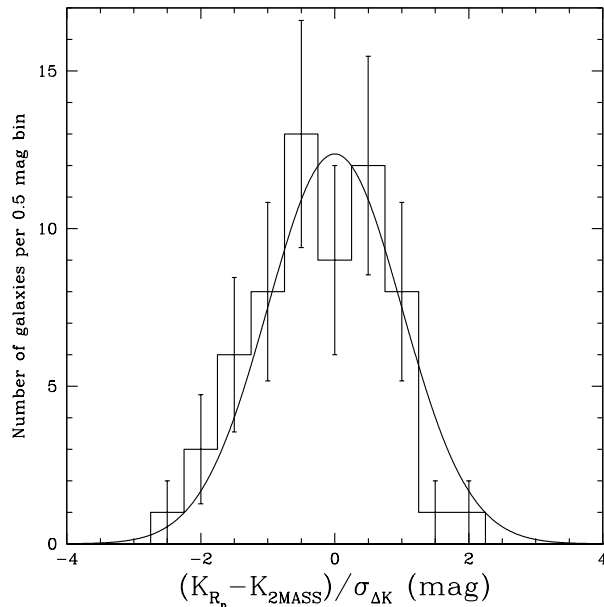


Figure 1. The histogram shows the distribution of the difference between our magnitudes obtained within twice the R-band Petrosian radius and the Kron elliptical magnitudes measured by 2MASS, normalised by the quadrature sum of the uncertainties on the two magnitudes ($\sigma_{\Delta K}$). The solid line shows a Gaussian distribution with unit standard deviation for comparison. This shows that our K magnitudes are consistent with those of 2MASS, within the uncertainties.

measured by 2MASS, for 56 galaxies. This difference is normalised by the quadrature sum of the uncertainties in the two magnitudes ($\sigma_{\Delta K}$), so the distribution should be a Gaussian with standard deviation of unity if the magnitudes are consistent within the errors. We include the systematic zeropoint uncertainty of 0.08 magnitudes on our UKIRT observations. The solid line shows this Gaussian curve for comparison; the data are fully consistent with this distribution, which shows that our fixed-metric apertures can be directly compared with the 2MASS Kron elliptical magnitudes. In absolute terms, the $1-\sigma$ standard deviation of the difference between the two magnitudes is 0.15 mag. The measured magnitudes are given in column 5 of Tables 1 and 2.

Luminosities are computed assuming a Λ CDM cosmology with the spectroscopic redshift from SDSS. No k-correction or evolution correction is applied to the luminosities or colours presented in this paper. This is because these corrections are model-dependent, and by their nature the galaxies in this sample may have unusual star formation histories which make the usual models inapplicable. Instead, we will compare samples within the same, relatively narrow, redshift ranges.

2.3.2 Morphology measurements

Galaxy morphologies are determined by fitting a two-dimensional parametric model to the surface brightness distribution, using the GIM2D software (Simard et al. 2002). The model consists of a bulge and disk component, and is completely described by twelve parameters. From these fits, we derive the ratio of the bulge luminosity to the total luminosity, B/T . Since the small UFTI field of view does not generally contain enough stars to obtain a reliable point-spread function (PSF) for each image, we use the PSF from the standard star observed most closely in time (generally within

2 hours). We find no significant correlation between the measured B/T and the seeing or redshift, from which we conclude that uncertainties in the PSF do not significantly influence our B/T measurements. The measured B/T values are given in column 6 of Tables 1 and 2. The formal uncertainties in B/T computed by GIM2D are quite small, < 0.1 ; however, the true uncertainty is likely to be dominated by systematic errors (such as PSF fitting and the assumption of a $r^{1/4}$ law for the bulge) on the order of ~ 0.1 – 0.2 . We also note that the B/T will be meaningless in irregular systems of close pairs or merging galaxies.

In Appendix A we show images and the corresponding surface brightness fits for most¹ of the galaxies in our sample, grouped by B/T and emission line strength (Figures A1–A8). For each galaxy we show the central $12''$ of the original K -band image, as well as the GIM2D best-fit model (with logarithmically spaced contours), and the residuals between the two. A visual comparison shows that the GIM2D B/T ratio provides a reasonable morphological classification; the low B/T galaxies mostly have obvious disks, while the high B/T galaxies are generally spheroidal. The method clearly does not deal well with galaxies that are distorted or have twisted isophotes; however, most of the galaxies in our sample have a normal appearance.

We also visually inspect each image for obvious signs of interactions, and we mark any galaxy that shows the strong morphological distortion typical of tidal effects, or a close companion and some indication for tidal distortion, as a possible interacting system. Our images are not deep enough to search for low surface-brightness tidal features, however. Furthermore, the completeness of our list of interacting galaxies is uncertain without doing a careful analysis of how surface brightness dimming with redshift and differences in galaxy surface brightness profile alter the detection of these features (e.g. Yang et al. 2004). We therefore do not present a quantitative analysis of these potentially interacting galaxies in this paper.

2.4 Stellar population modelling

To help interpret our observations we use the Bruzual & Charlot (2003) population synthesis models. For our fiducial model we assume a Salpeter (1955) initial mass function with solar metallicity. We first verify that reasonable models are able to reproduce the colours of normal galaxies by comparing with the r -selected SDSS data in Figure 2. The simplest case is to compare a single-burst, dust-free model, evolved for a Hubble time (13.7 Gyr), with bright (i.e. high signal-to-noise) SDSS galaxies which have no detectable [OII] or $H\alpha$ emission lines. The model prediction is shown as the large, filled circle, and the data are the small points; the agreement is good, and improved if we include a range of abundances for the early type population: a model with lower metal abundance, 40 per cent of solar, yields bluer colours as indicated by the longer arrow. Dust extinction changes the colours in the other direction, as shown by the shorter arrow. This estimate is based on the two-component model of Charlot & Fall (2000), with a total optical depth of $\tau_v = 1$, of which 30 per cent arises from the ambient ISM and the remainder is due to molecular clouds. Thus younger, more massive stars are more heavily extinguished than the older stellar population.

¹ We show all of the k+a galaxies, but for the sake of brevity just a random subsample of 48 of the 57 k+a galaxies with weak emission, and 60 of the 94 e(a) galaxies.

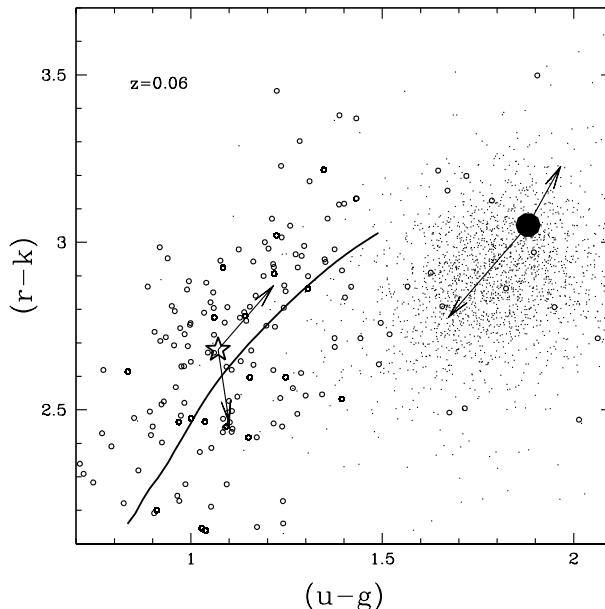


Figure 2. A colour-colour diagram of normal (r -selected) galaxies in the SDSS, compared with population synthesis models from Bruzual & Charlot (2003). These represent our fiducial models, which are intended to be representative of typical galaxies in the local Universe. The *small dots* are bright ($r < 16.4$) SDSS galaxies at $z = 0.06 \pm 0.01$ without strong emission lines ($W_o(H\alpha) < 2\text{\AA}$ and $W_o([OII]) < 2\text{\AA}$), while the *small, open circles* are galaxies at the same redshift and magnitude, but with $W_o(H\alpha) > 40\text{\AA}$ and $W_o([OII]) > 20\text{\AA}$. The *filled circle* shows a single-burst model, with no dust extinction, and a Salpeter (1955) initial mass function, after 13.7 Gyr of passive evolution. The smaller arrow (pointing to redder colours) shows the effect of increasing the dust optical depth from 0 to $\tau_v = 1$, with 30 per cent of the dust arising from the ambient ISM. The longer arrow (toward bluer colours) shows the effect of decreasing the metallicity to 40 per cent solar. The *large star* shows a model with constant star formation rate and dust extinction with a total optical depth $\tau_v = 1$. The redward arrow shows the effect of increasing the dust extinction to $\tau_v = 2$. The near-vertical arrow shows the effect of reducing the metallicity to 40 per cent solar. Finally, the *solid line* shows the evolutionary track of a galaxy with an exponentially declining SFR, with timescale 4 Gyr and $\tau_v = 1$.

To compare the model predictions for normal, star-forming galaxies we compute a model with a constant star formation rate over a Hubble time, and include dust extinction of $\tau_v = 1$, again assuming 30 per cent of the extinction arises from the ambient interstellar medium. This type of model is known to be a reasonable representation of local, star-forming galaxies (e.g. Brinchmann et al. 2004). The model is presented as the large star in Figure 2, and is compared with SDSS galaxies with $W_o(H\alpha) > 40\text{\AA}$ and $W_o([OII]) > 20\text{\AA}$ (open circles). Again the agreement is good, and the vectors show the effect of increasing the extinction to $\tau_v = 2$ or decreasing the metallicity to 40 per cent of solar. The solid line shows the evolutionary track of a galaxy with a SFR that declines exponentially, with a timescale of 4 Gyr, and $\tau_v = 1$; it nicely traces the locus of normal emission-line galaxies in the SDSS as it evolves over a Hubble time (from blue to red colours).

These models illustrate the usefulness of the $(u-g)$, $(r-k)$ colour combination. The $(u-g)$ colour is sensitive to population age (it differs by almost 1 magnitude between the two models), but is relatively weakly sensitive to metallicity and, especially, dust effects. On the other hand, the $(r-k)$ colours are approximately equally sensitive to age, metallicity and dust.

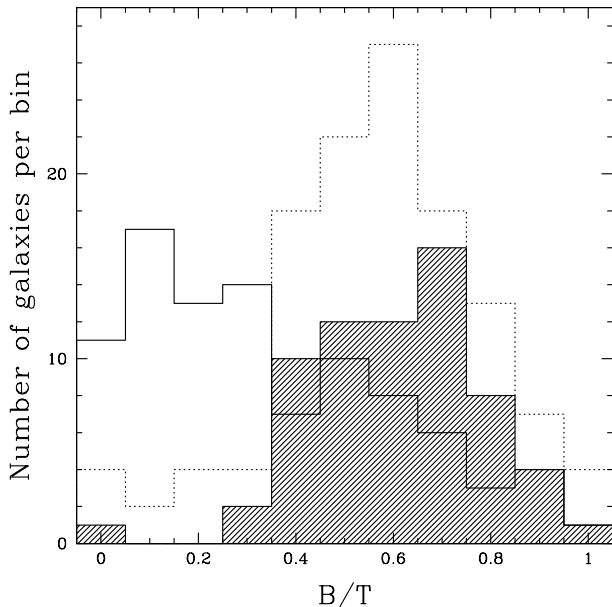


Figure 3. The distribution of B/T for the k+a galaxies (*shaded histogram*) and e(a) galaxies (*solid line*). The *dotted line* shows the result of adding galaxies with only weak emission lines ($W_o(\text{H}\alpha) < 10\text{\AA}$, $W_o([\text{OII}]) < 10\text{\AA}$) to the k+a sample. The distributions of k+a and e(a) galaxies are distinctly different, in the sense that k+a galaxies are primarily bulge-dominated, while e(a) galaxies are mostly disk-dominated.

3 RESULTS

3.1 Galaxy morphologies

Figure 3 shows the distribution of B/T for the k+a and e(a) galaxies in the sample. The two types of galaxies have distinctly different morphologies (significant at the $> 3\sigma$ level): while almost all the k+a galaxies are bulge-dominated, the opposite is true for e(a) galaxies. Similar results have been found by (Quintero et al. 2004), based on measurements of the Sersic profiles rather than B/T ratios. Including galaxies with weak emission ($W_o(\text{H}\alpha) < 10\text{\AA}$, $W_o([\text{OII}]) < 10\text{\AA}$) in the k+a sample does not change this result. Thus, galaxy morphology is correlated more strongly with the instantaneous star formation rate (i.e. emission lines) than with recent star formation over the last ~ 1 Gyr as represented by the H δ absorption line.

A closer examination of the disk-dominated k+a galaxies in Figure A1 shows that most have a very smooth disk component, with little or no evidence for spiral structure in the model residuals. This contrasts with the e(a) disk-dominated galaxies shown in Figure A7, which show morphologies more akin to typical spiral galaxies. The spheroid-dominated k+a galaxies appear mostly normal, with few signs of disturbance or interactions, although our data are not deep enough to identify the subtle features expected from recent merger activity (Yang et al. 2004).

3.2 Environment

We can characterize the galaxy environment by the number of neighbouring galaxies (e.g. Dressler 1980). Specifically, we measure Σ_5 , the density derived from the projected distance to the fifth-nearest neighbour brighter than $M_r = -20$, as in Balogh et al. (2004). This gives a useful estimate of the local density for galaxies at $z \lesssim 0.1$; at higher redshifts the spectroscopic limit is brighter

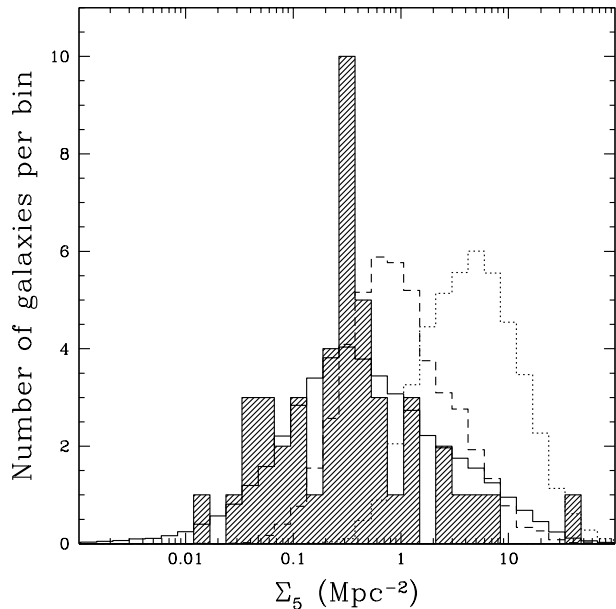


Figure 4. The distribution of projected local surface density Σ_5 for the k+a population at $0.05 < z < 0.1$ (*shaded histogram*, including galaxies with weak emission lines) compared with the r -selected SDSS subsample in the same redshift range (*solid line*). The remaining lines show the SDSS distribution restricted to galaxies in clusters with $\sigma > 400 \text{ km s}^{-1}$: the *dashed line* represents galaxies within $1 < R/R_{\text{vir}} < 3$ and the *dotted line* represents galaxies with $R < R_{\text{vir}}$, where R_{vir} is the cluster virial radius. The k+a galaxies are found in typical environments, and not preferentially in or near clusters.

than $M_r = -20$, and Σ_5 is therefore an underestimate. We therefore restrict our sample to galaxies in the redshift range $0.05 < z < 0.1$.

In Figure 4 we show the distribution of Σ_5 for the 46 k+a galaxies (including those with weak emission) in the redshift range $0.05 < z < 0.1$, compared with the distribution for all galaxies in that redshift range from the SDSS data (including those without available infrared magnitudes from 2MASS). The two distributions are statistically consistent with being drawn from the same population. Thus, k+a galaxies at $0.05 < z < 0.1$ are not more likely to be found in clusters than the typical r -selected galaxy in the SDSS. For comparison, we also show the distribution of Σ_5 for the subset of the SDSS galaxies found in clusters with velocity dispersion $\sigma > 400 \text{ km s}^{-1}$. The clusters are selected from the C4 catalogue of Miller et al. (2005), and we divide the galaxies into two populations based on their projected position relative to the cluster virial radius, R_{vir} . In the virialised regions of clusters, $r < R_{\text{vir}}$, densities are typically $\Sigma_5 \gtrsim 2 \text{ Mpc}^{-2}$, much larger than the densities of all but a few of our k+a galaxies. Even when considering only galaxies well outside the virial radius of these clusters, $1 < R/R_{\text{vir}} < 3$, local densities are typically ~ 3 times larger than average, and inconsistent with the k+a galaxy population. We therefore confirm the conclusions of others (Zabludoff et al. 1996; Quintero et al. 2004; Blake et al. 2004), that nearby k+a galaxies do not preferentially reside within clusters and rich groups; moreover, they are not more likely to be found in these dense environments than typical, r -selected galaxies.

Although k+a galaxies are found in both high and low density regions, it is interesting to investigate whether those few that are found in clusters differ in any significant way from the rest of the population. In Figure 5 we show the B/T ratio of the galaxy

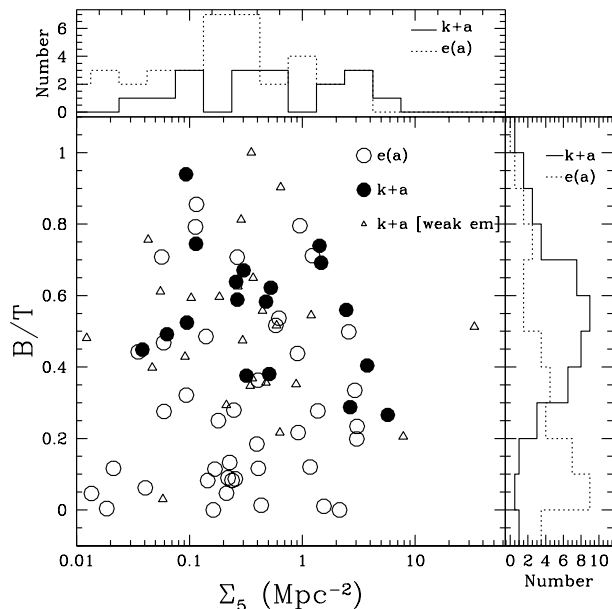


Figure 5. The morphologies of galaxies with $0.05 < z < 0.1$ are shown as a function of their local galaxy density. The *open circles* show the e(a) galaxies, while the *solid circles* represent the k+a galaxies. *Triangles* are k+a galaxies with a small amount of emission, $W_o(\text{H}\alpha) < 10\text{\AA}$ and $W_o([\text{OII}]) < 10\text{\AA}$. The histograms on the top and left of the figure show the collapsed distributions of Σ_5 and B/T for the k+a galaxies (including those with weak emission) and e(a) galaxies, as indicated. Although k+a and e(a) galaxies are found in similar environments, their morphologies are distinctly different.

sample with $0.05 < z < 0.1$, as a function of Σ_5 . The small sample means that it is difficult to robustly identify any trends with environment, and a Spearman’s rank correlation test does not find a significant correlation. However, we note that in the densest regions, $\Sigma_5 > 2 \text{ Mpc}^{-2}$, we do not find any galaxies with $B/T > 0.6$. Although this difference is not statistically significant, neither can we rule out the possibility that k+a galaxies in clusters are mostly disk-dominated (e.g. Tran et al. 2003; Caldwell et al. 1996), and are a distinct phenomenon from the bulge-dominated galaxies in the field.

The e(a) galaxies, while morphologically quite distinct from the k+a galaxies, inhabit similar environments. The distributions and sample means of Σ_5 for the two populations are statistically consistent with being drawn from the same population, as determined with a Kolmogorov–Smirnov test and a Student’s t-test, respectively. Thus the difference between these two types of galaxy does not appear to be related to environment.

3.3 Optical and infrared magnitudes

The photometric data are presented as a colour–magnitude diagram in Figure 6, where we compare the optical (u-g) colours of our sample with the UKIRT k magnitudes, in four redshift bins. For comparison we also show as small dots those SDSS galaxies with $W_o(\text{H}\alpha) < 4\text{\AA}$, for which a K-band magnitude is available from the shallower 2MASS. Our r-selected e(a) and k+a galaxies have k magnitudes as faint as $k \sim 15$, well below the 2MASS limit. Because the sample is magnitude-limited, the luminosity distribution is strongly redshift-dependent. We show the characteristic magnitude K^* from Cole et al. (2001), $M = -24.2$, at the midpoint of

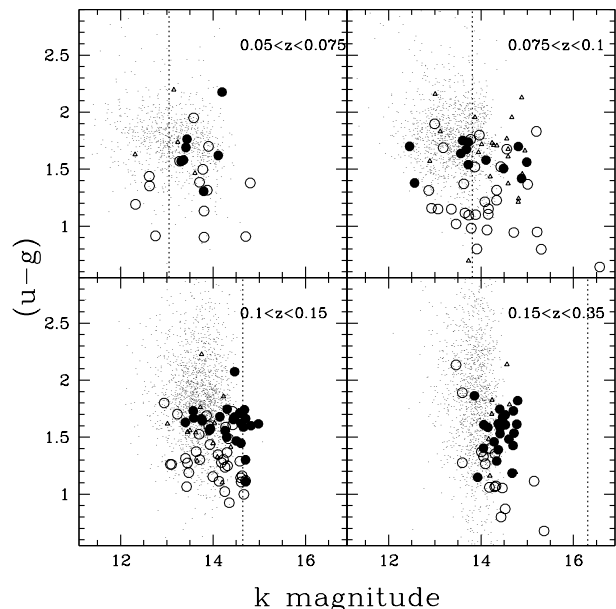


Figure 6. The observed (u-g) colours as a function of k magnitude for the k+a galaxies (*filled circles*) and e(a) galaxies (*open circles*). *Triangles* represent k+a galaxies with weak emission lines. The *small dots* are normal SDSS galaxies for which K-magnitudes are obtained from 2MASS, and which show no $\text{H}\alpha$ emission ($W_o(\text{H}\alpha) < 4\text{\AA}$). We only show a random 10 per cent of the galaxies for clarity. The *dotted lines* show the characteristic luminosity $M^* = -24.2$ from Cole et al. (2001), neglecting small k and evolution-corrections. Our magnitude selection effect means the nearby galaxies are mostly faint, while the highest redshift sample includes only the most luminous galaxies.

each redshift bin, neglecting k- and evolution-corrections, which are small for normal galaxies (generally $< 0.2 \text{ mag}$). In our highest redshift bin ($z > 0.15$), which contains ~ 30 per cent of the sample, the galaxies are very luminous, $\sim 1.5 \text{ mag}$ brighter than L^* . On the other hand, at the lowest redshifts, $0.05 < z < 0.075$, all seven of the k+a galaxies observed are fainter than K^* , by up to $\sim 1 \text{ mag}$. Note that this is consistent with the results of Poggianti et al. (2004) who find that the k+a population in Coma consists mostly of faint galaxies. However, the lack of brighter galaxies in our small low-redshift sample is only inconsistent with the normal, passive galaxy distribution at the 2σ level. Most of the k+a and e(a) galaxies are bluer in (u-g) than the red sequence of typical SDSS galaxies lacking $\text{H}\alpha$ emission. This is not surprising, since the e(a) galaxies have emission lines indicative of ongoing star formation, and the strong $\text{H}\delta$ absorption of the k+a galaxies likely indicates recent star formation activity.

4 INTERPRETATION AND MODELLING

4.1 Optical and infrared colours

We show the optical–infrared colour ($r-k$) as a function of (u-g) in Figure 7. The solid line in the figure is the normal spiral evolution track introduced in Figure 2; it is evident that most of the e(a) galaxies lie along this locus. The tightness of the colour relation is surprising, and may break down at the highest redshifts, $z > 0.15$, where unfortunately our sample of e(a) galaxies is small. It is also noteworthy that many e(a) galaxies lie redward of the end of the normal spiral track (and redder than normal star-forming galaxies;

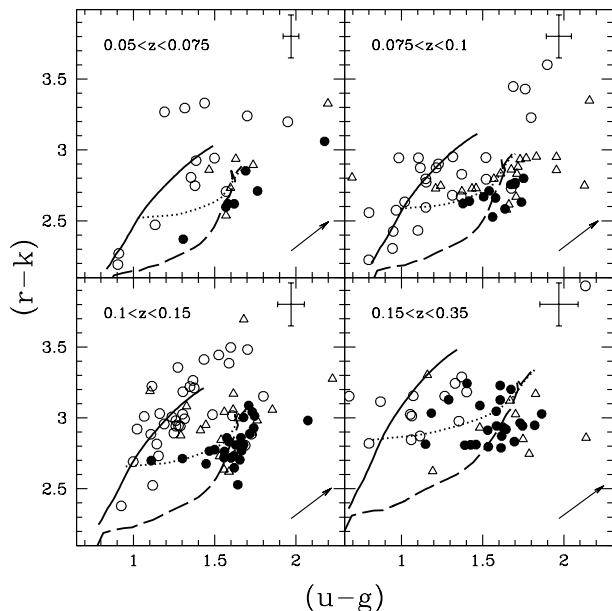


Figure 7. The $(u-g)$ - $(r-k)$ colour-colour diagram in four redshift bins. The *open circles* represent the e(a) galaxies, and the *filled circles* are the k+a galaxies; *triangles* represent k+a galaxies with some weak emission. The sample error bars in the top right of each panel show the median 1σ uncertainties. The lines show three different models from Bruzual & Charlot (2003), as described in the text. The arrow in the bottom-right of each panel shows the change in colour corresponding to dust extinction of $\tau_v = 1$. The *solid line* shows a galaxy with $\tau_v = 1$ and an exponentially declining star formation rate, with $\tau = 4$ Gyr; colours become redder with time. The *dotted line* shows the effect of truncating star formation in a galaxy that was forming stars at a constant rate for 13.7 Gyr (i.e. a Hubble time). The *dashed line* shows the evolution of a galaxy with an old stellar population after the addition of a burst accounting for 15 per cent of its stellar mass. Evolution is from left to right, and both models assume no dust extinction. Further details on the models are given in the text. The k+a and e(a) galaxies are distinctly separate populations in this plane, and generally inconsistent with the truncated-star formation model (dashed line).

recall Figure 2), in the direction expected if they are more than normally reddened by dust.

In contrast, the k+a galaxies have colours that are distinct from those of most normal galaxies in general, and e(a) galaxies in particular. In particular, they have $(u-g)$ colours that are intermediate between the passive and star-forming population, as we saw in Figure 6, while their $(r-k)$ colours are similar to those of the normal star-forming population. Note also that galaxies with only weak emission (the triangles in the figure) have colours most similar to the k+a population, rather than the e(a) population or something in between the two.

To interpret these colour distributions, we consider two distinct variations on the normal galaxy models introduced in § 2.4. It is not our goal to explore the full range of parameter space; degeneracies with dust, initial mass function, and metallicity make it difficult to make robust statements about the star formation history. However, we will contrast two very different models as an illustration of the two broad paths generally proposed to generate a k+a spectrum: either truncating star formation in a normal disk galaxy, or introducing a short burst of star formation on an older population. We model the first case (“truncation”) by taking a galaxy with a constant star formation rate and truncating star formation after a Hubble time (13.7 Gyr, at which point the integrated

colours are similar to those of normal spiral galaxies); this model is shown as the dotted line in Figure 7. We assume no dust extinction in this model, based on the assumption that even if the initial galaxy has substantial dust, the termination of star formation (whether by merger-induced starbursts or gas stripping, for example) would be accompanied by a depletion of dust as well. At the time when star formation ceases, the model quickly becomes redder in the star-formation sensitive $(u-g)$ colour; however the $(r-k)$ colour remains approximately constant. Approximately 300 Myr later, $(r-k)$ also begins to redden. Furthermore, the $(u-g)$ colour evolution slows down: it takes ~ 1.4 Gyr for $(u-g)$ to redden by only another 0.2 magnitudes. The observed population of k+a galaxies (and a few e[a] galaxies) have $(u-g)$ colours that are similar to this transition point, a few hundred Myr after the truncation of star formation; however, the $(r-k)$ colours of many are too blue. This is a generic problem of the assumption that the galaxy starts from a colour that is typical of normal spiral galaxies, since $(r-k)$ can only get redder after the truncation of star formation, and including dust extinction in the model makes the situation worse. The only way to match the $(r-k)$ colours with this kind of model is to start with a bluer galaxy, initially, than a galaxy with a constant star formation rate. One way to do this would be with a current (or very recent) star formation rate that exceeds its past average; this becomes a weaker version of the “starburst” model considered below. We can therefore conclude that the $(r-k)$ colours of many k+a galaxies are inconsistent with the assumption that they form via the truncation of star formation in normal spiral galaxies.

To investigate the alternative case, we start with an evolved (13.7 Gyr), dust-free, single burst population, which has colours typical of the red locus of SDSS galaxies. We then add a burst comprising 15 per cent of the total mass of stars formed and evolve the model for another 2 Gyr; this is shown as the dashed line (which starts from the end of the burst and evolves redward). In this case, the colour evolution provides an excellent match to the average colours of most k+a galaxies. We cannot draw strong conclusions regarding the strength or age of the burst based on these data, however. Even for this particular choice of parameters (i.e. metallicity, dust, initial mass function) the scatter in the colours admits any burst strength > 5 per cent.

It is evident is that the e(a) population in general does not lie along either model track: their colours resemble normal spiral galaxies more than they do an early phase of the k+a galaxies. This is at least true for all but the highest redshift galaxies in our sample. At $z > 0.15$ the e(a) and k+a populations may be more consistent with a single colour sequence, approximately following the truncated spiral galaxy model. However, there are few data here, and they span a significant redshift range which will increase the scatter in the colours. If the difference relative to the lower redshift bins is real, it may be an evolutionary effect, or it may be a luminosity effect, as the highest redshift k+a and e(a) galaxies are up to ~ 3 magnitudes more luminous (and therefore likely more metal-rich) than their low-redshift counterparts.

4.2 Colours and $H\delta$ line strengths

In Figure 8 we show the observed and model dependence of $H\delta$ line strength on $(u-g)$ and $(r-k)$ colour. The models are the same ones presented in Figure 7. In order to make the comparison between the models and data fair, the line strengths for both are remeasured following the definition of Worthey & Ottaviani (1997). These measurements differ from the more sophisticated measurements of Goto et al. (2003), which are based on a model

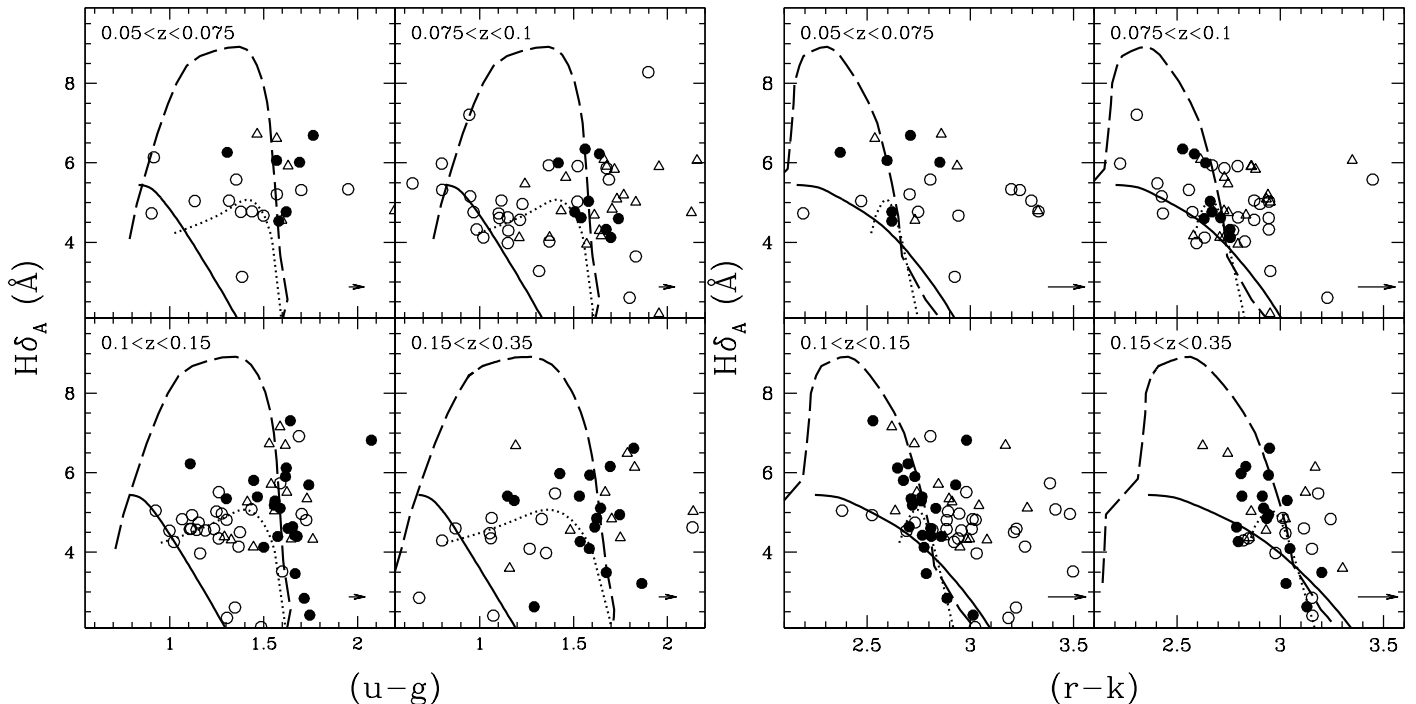


Figure 8. The $H\delta$ line strength, defined as in Worthey & Ottaviani (1997), is shown as a function of $(u - g)$ colour (left) and $(r - k)$ colour (right). The open symbols are the e(a) galaxies, and the solid circles are k+a galaxies. Triangles are k+a galaxies with a small amount of nebular emission. The lines show the same models as in Figure 7, and the arrow in the lower right corner shows the effect of increasing the dust extinction by 1 magnitude in a galaxy with a constant star formation rate. Note that the $H\delta_A$ predictions for the normal spiral model (solid line) are upper limits, as emission-filling will reduce the equivalent width. The k+a galaxies show good agreement with the burst model (dashed line), while many of the e(a) galaxies are particularly noteworthy for their very red $(r - k)$ colours, suggestive of strong dust obscuration.

Gaussian fit to the data; to distinguish them we adopt the notation of Worthey & Ottaviani (1997) and label them $H\delta_A$. In general the two measurements are comparable, but there are a few cases where the Worthey & Ottaviani (1997) definition yields a significantly lower value. The original Goto et al. (2003) measurements are given in column 7 of Tables 1 and 2, while our remeasured $H\delta_A$ are listed in column 8. For completeness, the rest-frame equivalent widths of [OII] and $H\alpha$ from the SDSS pipeline are also given in those tables as columns 9 and 10, respectively.

As has been noted many times before (e.g. Couch & Sharples 1987; Poggianti et al. 1999; Balogh et al. 1999), truncating star formation in a normal spiral galaxy (i.e. one that has been forming stars at a constant rate for many Gyr) does not produce strong enough $W_o(H\delta)$ to match the strongest-lined k+a galaxies. However, the relatively narrow colour range of most of the k+a galaxy population is in remarkably good agreement with the 15 per cent burst model, for the range of observed $W_o(H\delta)$ strengths. The galaxies with the strongest $H\delta$ lines are the most convincing: only the burst model can match the relatively red $(u - g)$ colours and the blue $(r - k)$ colours, simultaneously with the strength of the absorption. Again the burst strength is not well constrained, and any burst making up at least 5 per cent of the stellar mass is in agreement with most of the data.

On the other hand, the e(a) galaxies show a large amount of scatter, and do not appear to form a single sequence. Some of this scatter will be caused by emission-filling of $H\delta$ absorption, which is not accounted for, and means that $H\delta_A$ is an underestimate of the underlying absorption. Although in many cases the $(u - g)$ colours and $H\delta$ line strengths are approximately consistent with the truncated spiral model, the $(r - k)$ colours are much too red for this

to be the correct model (also, of course, the presence of emission lines in the spectrum means a completely truncated model cannot be physically correct). In fact, the $(r - k)$ colours of the reddest galaxies are not matched by any of the models presented here; since this colour is much more sensitive to dust extinction than $(u - g)$, one possible interpretation is that e(a) galaxies are more heavily extinguished than normal spirals. For most of the population an extra ~ 1 magnitude of dust extinction would be consistent with their position on the colour-colour diagram of Figure 7. Conversely, the lack of scatter in $(r - k)$ colour for the k+a population means that dust is unlikely to play a strong role in the spectral properties of these galaxies.

4.3 Stellar luminosities and masses

The K -band luminosity is a good tracer of stellar mass, and is less sensitive to the recent star formation history than optical luminosities. However, the M/L_K ratio can still vary by a factor ~ 2 depending on population age; in Figure 9 we show how M/L_K depends on $(u - g)$ and $(r - k)$ colour for the models considered in this paper. The fiducial model of an old galaxy population, presented in Figure 2, has $M/L_K \sim 1.15$, while the constant star-formation model (with $\tau_v = 1$ dust extinction) has $M/L_K \sim 0.55$. Thus, the bluest normal galaxies are typically a factor ~ 2 less massive than red galaxies of the same K -luminosity. Our best interpretation for most of the e(a) population is that they are normal (though possibly dusty) spiral galaxies, which means they will also have $M/L_K \sim 0.55$. We also show the models of truncated star formation in a normal disk galaxy, and of a 15 per cent burst superposed on an old stellar population. Recall that this latter model

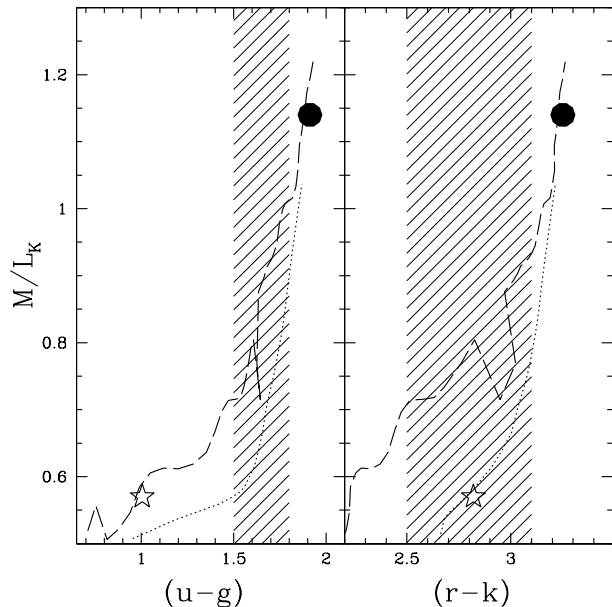


Figure 9. The M/L_K ratio for four Bruzual & Charlot (2003) models at $z = 0.12$, as a function of $(u - g)$ colour (left) or $(r - k)$ colour (right). The *solid circle* and *large star* represent the old and young fiducial models, as presented in Figure 2. The *dotted line* shows the truncated-disk model, where star formation is abruptly stopped after 13.7 Gyr and there is no dust. The *dashed line* shows the track for a 15 per cent burst of star formation on top of an old stellar population, also without dust. The *shaded region* shows approximately the colour range of observed k+a galaxies at $0.1 < z < 0.15$, from Figure 7. If typical k+a galaxies result from a 15 per cent burst superposed on an old stellar population, this indicates they will have $M/L_K \sim 0.8 \pm 0.1$.

provides a good match to the colours, H δ line strengths, and morphologies of the k+a population, but the burst strength is poorly constrained only to be > 5 per cent by mass. This model predicts $M/L_K \sim 0.8 \pm 0.1$ at the colours typical of the k+a galaxies at $z \sim 0.12$, not too dissimilar from the value one would obtain by interpolating between the evolved and star-forming models, as a function of $(u - g)$. Thus, if the model we have chosen to represent the colours of k+a galaxies is correct, then they have ~ 75 per cent of the mass of normal, passive galaxies at the same K-band luminosity. The typical M/L_K will be higher, $\sim 1 \pm 0.1$ if the burst only makes up 5 per cent of the final mass, and more consistent with the M/L_K of normal passive galaxies.

5 DISCUSSION

5.1 The connection between e(a) and k+a galaxies

The observations and modelling results presented in this paper suggest that most e(a) galaxies are not directly related, in an evolutionary sense, to k+a galaxies. This conclusion is based primarily on the fact that, although the range of H δ absorption strengths are similar, the colours and infrared morphologies of the two populations are quite distinct. In particular, the insensitivity of K luminosity to recent star formation provides a strong morphological argument against the interpretation that k+a galaxies arise following the end of star formation in e(a) galaxies. From Figure 3 we saw that most k+a galaxies have $B/T \sim 0.6$, while most e(a) galaxies have $B/T \sim 0.1$. If we assume that all star formation occurs in the disk component, then a termination of star formation means the disk will

fade by only a factor ~ 2 (Figure 9). Thus the typical e(a) galaxy that started with $B/T = 0.1$ would end up with $B/T = 0.18$, where the disk is still much more prominent than for typical k+a galaxies. Conversely, to reproduce the typical morphology of k+a galaxies through disk fading, the progenitor would have to have $B/T = 0.42$. Therefore this simple fading mechanism cannot connect the two different morphological distributions, and this conclusion is only strengthened if some of the star formation takes place in the bulge, rather than the disk (e.g. Norton et al. 2001). Although this conclusion holds for about half the e(a) population, we note that the distribution of e(a) morphologies includes a significant tail extending to bulge-dominated systems, which are morphologically consistent with being progenitors of k+a galaxies.

The colours of most e(a) galaxies are sufficiently red that it is unlikely their colours will evolve to match those of k+a galaxies once star formation stops. This does not mean that none of the e(a) galaxies will evolve into k+a types; the bluest ~ 10 per cent of the population may be starburst systems that could represent k+a progenitors. However, most of these blue e(a) galaxies still have disk-dominated morphologies, as shown in Figure A6. It is possible that a subsequent merger event could destroy this disk, and in fact, about half of the bluest e(a) galaxies show some suggestive evidence for interaction with a nearby companion. However, it is not clear if this abundance of interactions is better correlated with galaxy colour or H δ line strength, so we cannot conclude that the e(a) spectrum is a unique characteristic of interacting systems destined to become k+a galaxies. Finally, we note that if the colours of e(a) galaxies are the result of unusually strong dust obscuration, then more of them will have blue intrinsic colours; as long as the dust is destroyed with the cessation of star formation (for example, in a starburst), their colours might evolve to be consistent with those of k+a galaxies.

Although we conclude that e(a) galaxies are not all progenitors of k+a galaxies, we note that the argument does not work in reverse. It is possible that the progenitors of today’s k+a population all had an e(a) spectrum in the past. These progenitors would have to be either a subset of the e(a) galaxies observed today (those that are blue and disk-dominated) or perhaps an entirely different population of very blue e(a) galaxies that are so short-lived they are not present in our sample. However it seems likely that selection based on H δ strength alone is not an efficient way to find the progenitors of k+a galaxies.

We will consider the mass function of k+a and e(a) galaxies in a subsequent paper; here we present just the observed distribution of K-band luminosities, uncorrected for selection effects, to ensure that our comparisons of the two populations are based on samples of similar stellar masses. In Figure 10 we show the luminosity distributions in solar units, using $K_{\odot} = 3.33$ (Cox 2000), neglecting k- and evolutionary corrections. We include galaxies with weak emission lines in the k+a sample. From the mass-to-light ratio calculation computed above we see that the mode of our k+a sample is at $M \sim 8 \times 10^{10} M_{\odot}$; for the e(a) galaxies (which we interpret as normal spiral galaxies) the mode is only 25 per cent lower, at $M \sim 6 \times 10^{10} M_{\odot}$. This only shows that when comparing the two types of galaxies we are comparing objects of similar mass; of course the shape of the distributions are heavily biased by our selection function.

5.2 Comparison with previous work

Our data are most consistent with the interpretation that local k+a galaxies are a short-lived phase that occurs following a starburst

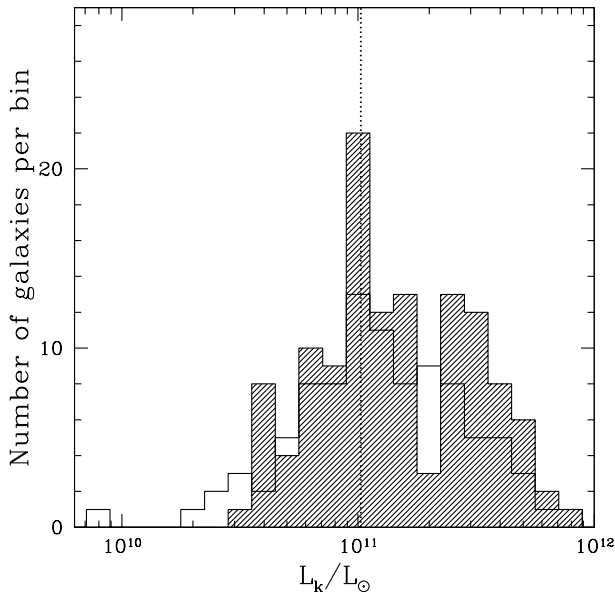


Figure 10. The K luminosity distribution, in solar units, of the k+a galaxies (*shaded histogram*, including galaxies with weak emission lines) and the e(a) galaxies (*solid histogram*). This is just the observed distribution of the sample and is not corrected for magnitude (or other) selection effects. The two distributions are not significantly different, demonstrating that the observed differences in morphology and colours are not due to differences in luminosity. The *dotted line* shows the characteristic luminosity, from Cole et al. (2001), for reference.

in a spheroidal galaxy; a likely cause for such a burst is a recent merger event. Our results are generally consistent with those of Norton et al. (2001) and Yang et al. (2004), who find the dynamics and morphologies of local k+a galaxies are typical of early-type galaxies. These authors claim the origin is from the merger of two galaxies, at least one of which is gas-rich, based on tidal features in some galaxies (Zabludoff et al. 1996; Norton et al. 2001) (see also Swinbank et al. 2005). Although we do not see convincing evidence that a substantial fraction of our k+a galaxies are currently undergoing mergers, our images are not deep enough to see low surface brightness tidal features indicative of recent interactions.

The lack of bright, k+a galaxies in dense environments is consistent with the results of Poggianti et al. (2004), who find that k+a galaxies in Coma are mostly much fainter than L^* . However, our sample is too small to claim more than this consistency, due to the general rarity of bright galaxies and dense environments. In distant clusters, there is evidence that disk-dominated k+a galaxies may be more common (Tran et al. 2003), and therefore could arise through a different mechanism from the bright, field k+a galaxies studied here. Our results are not inconsistent with this interpretation, as the few k+a galaxies we find in dense environments do have $B/T < 0.6$; however, there are too few galaxies to provide strong evidence either way.

6 CONCLUSIONS

We have presented UKIRT K -band observations of 222 galaxies selected from the SDSS first data release based on their strong $H\delta$ absorption, $W_o(H\delta) > 4\text{\AA}$. The purpose of this paper has been to use K -band luminosities as a tracer of total stellar mass and morphology to study the connection between $H\delta$ -strong galaxies

with e(a) and without (k+a) strong nebular emission (i.e. ongoing star formation). Our conclusions are the following:

- The k+a and e(a) galaxies have very different distributions of morphology (although there is overlap). The k+a galaxies are mostly spheroidal; where there is a disk, it tends to be smooth with little sign of spiral structure. On the other hand, most e(a) galaxies resemble normal spiral galaxies with a prominent disk and spiral structure. Thus morphology is more closely correlated with ongoing star formation (emission lines) than with recent star formation (Balmer absorption).
- The K -band fractional bulge luminosities of k+a galaxies are too large to result from the truncation of star formation in a typical e(a) or normal spiral galaxy.
- The k+a galaxies form a surprisingly tight sequence in $(u-g)$ and $(r-k)$ colour, and $H\delta$ line strength. A model of an old (13.7 Gyr), dust-free galaxy with a Salpeter initial mass function and a recent burst of star formation accounting for 15 per cent of its mass, traces the mean properties of this sequence well. However the burst strength is not well constrained; any value > 5 per cent is consistent within the scatter of the data. The lack of scatter in the dust-sensitive $(r-k)$ colours for these galaxies suggests that their unusual spectral appearance is not due to the effects of dust.
- The e(a) galaxies form a sequence in $(u-g)-(r-k)$ colour-colour space that is disjoint from the k+a sequence. Furthermore, the $(r-k)$ colours of most are too red for their $H\delta$ absorption to be accounted for by the same model that produces k+a galaxies. Instead, a consistent model for e(a) galaxies is that of a dust-reddened (by $\tau_V \sim 2$) but otherwise normal spiral galaxy. However, we have not searched for a unique model and other explanations may be admissible, including variations in the initial mass function.
- With the above interpretation, we can determine the M/L_K ratio for each type of galaxy. While $M/L_K \sim 0.55$ for the e(a) population, $M/L_K = 0.8 \pm 0.1$ for the k+a galaxies. This latter value depends on the assumption that the starburst accounts for 15 per cent of the stellar mass; a 5 per cent burst has only a small effect and the resulting $M/L_K \sim 1$ is not too different from normal, evolved stellar populations.
- Galaxies with strong $H\delta$ and a small amount of emission ($W_o([OII]) < 10\text{\AA}$ and $W_o(H\alpha) < 10\text{\AA}$) have colours and morphologies similar to those of k+a galaxies, and distinct from e(a) galaxies with stronger emission lines.
- Both e(a) and k+a galaxies are found in similar environments, as characterised by the number of bright neighbouring galaxies. The distribution of environments is typical of SDSS galaxies in general, and neither k+a nor e(a) galaxies are restricted to cluster cores or outskirts ($< 3R_{vir}$).

We therefore conclude that most e(a) and k+a galaxies are distinct populations, and arise in different ways. While most e(a) galaxies appear to be spiral galaxies with unusually high dust extinction (or perhaps an atypical initial mass function), most k+a galaxies are spheroidal galaxies with a recent, substantial (> 5 per cent by mass) burst of star formation. The progenitors of k+a galaxies may still have had an e(a) spectrum; these could either be the subset of present-day e(a) galaxies (the bluest examples with evidence of interactions), or a short-lived blue population that is not represented in our e(a) sample. However, most emission line galaxies selected on $H\delta$ and r -magnitude alone are unlikely to be progenitors of k+a galaxies.

ACKNOWLEDGEMENTS

We thank the observers who carried out our queue observations at UKIRT in semester 03A: S. Littlefair, Ian Smail, R. Jameson, David Gilbank, J. Dunlop, Sandy Leggett and Watson Varricatt.

REFERENCES

- Abazajian K., et al., 2003, *AJ*, 126, 2081
 Abazajian K., et al., 2004, *AJ*, 128, 502
 Abraham R. G., Smecker-Hane T. A., Hutchings J. B., Carlberg R. G., Yee H. K. C., Ellingson E., Morris S., Oke J. B., Rigler M., 1996, *ApJ*, 471, 694
 Baldry I. K., Glazebrook K., Brinkmann J., Ivezić Z., Lupton R. H., Nichol R. C., Szalay A. S., 2004, *ApJ*, 600, 681
 Balogh M. L., Baldry I. K., Nichol R. C., Miller C., Bower R. G., Glazebrook K., 2004, *ApJL*, 615, L101
 Balogh M. L., Morris S. L., 2000, *MNRAS*, 318, 703
 Balogh M. L., Morris S. L., Yee H. K. C., Carlberg R. G., Ellingson E., 1999, *ApJ*, 527, 54
 Barger A. J., Aragon-Salamanca A., Ellis R. S., Couch W. J., Smail I., Sharples R. M., 1996, *MNRAS*, 279, 1
 Barnes J. E., 1992, *ApJ*, 393, 484
 Bartholomew L. J., Rose J. A., Gaba A. E., Caldwell N., 2001, *AJ*, 122, 2913
 Blake C., et al., 2004, *MNRAS*, 355, 713
 Brinchmann J., Charlot S., White S. D. M., Tremonti C., Kauffmann G., Heckman T., Brinkmann J., 2004, *MNRAS*, 351, 1151
 Bruzual G., Charlot S., 2003, *MNRAS*, 344, 1000
 Caldwell N., Rose J. A., Franx M., Leonardi A. J., 1996, *AJ*, 111, 78
 Castander F. J., Nichol R. C., Merrelli A., the Sloan collaboratio 2001, *AJ*, 121, 2331
 Chang T., van Gorkom J. H., Zabludoff A. I., Zaritsky D., Mihos J. C., 2001, *AJ*, 121, 1965
 Charlot S., Fall S. M., 2000, *ApJ*, 539, 718
 Cole S., Norberg P., Baugh C. M., Frenk C. S., et al., 2001, *MNRAS*, 326, 255
 Couch W. J., Sharples R. M., 1987, *MNRAS*, 229, 423
 Cox A. N., 2000, *Allen's astrophysical quantities*. New York: AIP Press; Springer
 Dressler A., 1980, *ApJ*, 236, 351
 Dressler A., Gunn J. E., 1982, *ApJ*, 263, 533
 Dressler A., Gunn J. E., 1992, *ApJS*, 78, 1
 Dressler A., Smail I., Poggianti B. M., Butcher H., Couch W. J., Ellis R. S., Oemler A. J., 1999, *ApJS*, 122, 51
 Galaz G., 2000, *AJ*, 119, 2118
 Goto T., Nichol R. C., et al., 2003, *PASJ*, 55, 771
 Jarrett T. H., Chester T., Cutri R., Schneider S., Skrutskie M., Huchra J. P., 2000, *AJ*, 119, 2498
 Liu C. T., Kennicutt R. C., 1995, *ApJ*, 450, 547
 Miller C. M., Nichol R. C., et al., 2005, *AJ*, in press
 Miller N. A., Owen F. N., 2001, *ApJL*, 554, L25
 Norton S. A., Gebhardt K., Zabludoff A. I., Zaritsky D., 2001, *ApJ*, 557, 150
 Poggianti B. M., Bridges T. J., Komiyama Y., Yagi M., Carter D., Mobasher B., Okamura S., Kashikawa N., 2004, *ApJ*, 601, 197
 Poggianti B. M., Smail I., Dressler A., Couch W. J., Barger A. J., Butcher H., Ellis R. S., Oemler A. J., 1999, *ApJ*, 518, 576
 Poggianti B. M., Wu H., 2000, *ApJ*, 529, 157
 Quintero A. D., Hogg D. W., Blanton M. R., Schlegel D. J., Eisenstein D. J., Gunn J. E., Brinkmann J., Fukugita M., Glazebrook K., Goto T., 2004, *ApJ*, 602, 190
 Salpeter E. E., 1955, *ApJ*, 121, 161
 Schlegel D. J., Finkbeiner D. P., Davis M., 1998, *ApJ*, 500, 525
 Simard L., Willmer C. N. A., Vogt N. P., Sarajedini V. L., Phillips A. C., Weiner B. J., Koo D. C., Im M., Illingworth G. D., Faber S. M., 2002, *ApJS*, 142, 1
 Smail I., Morrison G., Gray M. E., Owen F. N., Ivison R. J., Kneib J.-P., Ellis R. S., 1999, *ApJ*, 525, 609
 Springel V., 2000, *MNRAS*, 312, 859
 Strateva I., Ivezić Ž., et al., 2001, *AJ*, 122, 1861
 Swinbank M., Balogh M., Bower R., Hau G., Allington-Smith J., Nichol R., Miller C., 2005, *ApJ*, 622, 260
 Tran K. H., Franx M., Illingworth G., Kelson D. D., van Dokkum P., 2003, *ApJ*, 599, 865
 Worthey G., Ottaviani D. L., 1997, *ApJS*, 111, 377
 Yang Y., Zabludoff A. I., Zaritsky D., Lauer T. R., Mihos J. C., 2004, *ApJ*, 607, 258
 Zabludoff A. I., Zaritsky D., Lin H., Tucker D., Hashimoto Y., Shectman S. A., Oemler A., Kirshner R. P., 1996, *ApJ*, 466, 104

Table 1: The k+a galaxy sample and measured properties

RA (J2000)	Dec	z	r' (mag)	K_s	B/T	$W_o(H\delta)$	$H\delta_A$	$W_o(O[II])$ (Å)	$W_o(H\alpha)$
3.120312	-0.894937	0.128834	16.71	13.7	0.46	4.7	4.3	5.6	5.4
3.963556	-10.388311	0.198220	17.5	14.7	0.67	7.4	6	1.9	0
9.282578	0.410167	0.080655	17.11	14.3	0.35	5.5	5.5	7.5	2.5
17.773197	14.266232	0.099456	16.93	14.2	0.76	5.1	4.8	3.6	-
20.065346	-9.988923	0.136923	17.22	14.5	0.56	4.4	4.4	2	-
20.226444	13.765402	0.127631	16.54	13.5	0.76	5.5	5.2	5.9	5.3
26.196381	0.537470	0.178903	17.46	14.4	0.42	6.6	4.1	3	-
27.779242	-0.943535	0.198065	17.38	14.5	0.7	4.7	5.1	0.5	-
29.191742	-9.950396	0.126340	17.75	14.7	0.98	6.1	5.9	6.8	9.2
30.125355	-9.890063	0.095773	17.3	14.6	0.61	4.3	4.1	2.7	2.3
31.007927	14.241354	0.081300	17.5	14.6	0.4	5.3	5.2	3	2.1
36.112850	-9.627632	0.088286	17.01	14.3	0.48	5.2	4.8	3.9	-
36.930046	-0.256401	0.219166	16.74	13.9	0.74	5.3	5.4	2	1.2
37.078602	-1.034778	0.091273	17.42	14.6	0.8	5.1	4.7	7.5	-
37.489056	-0.903572	0.085923	17.18	14.2	0.43	5.6	5.1	3.1	3.7
38.693249	0.509964	0.140466	17.28	14.6	0.8	6.1	5.8	2.2	-
39.761936	-0.530933	0.136121	17.45	13.8	0	4.7	1.9	7	-
45.830013	-8.605536	0.075652	16.77	14.1	0.52	4.9	5	1.1	-
46.116833	-8.818506	0.119705	17.25	14.6	0.46	6.3	6.1	1.9	-
47.029408	0.456219	0.074281	15.25	12.3	0.81	5.9	5.9	2.8	8.5
51.094597	-5.940036	0.204436	17.59	14.5	1	6.4	5.5	3.8	3.3
60.141998	-6.407394	0.179402	16.89	13.9	0.7	5.1	3.2	1	-
113.390167	37.834980	0.096724	17.45	14.6	0.36	5.6	5.9	3.8	1.1
113.905518	39.562695	0.108367	16.69	13.9	N/A	5.4	5.3	1.3	-
118.233299	38.725178	0.126291	17.53	14.7	0.7	4.7	4.1	2.9	-1.1
124.110924	41.562134	0.101673	17.29	14.2	0.6	5.1	-1.7	4.6	-
126.852570	51.797470	0.081440	16.44	13.7	0.74	4.7	4.6	1.8	-
127.648438	49.455341	0.132265	16.21	13.4	0.92	4.7	4.6	0.7	-
128.130447	49.411301	0.183051	17.24	14.4	0.43	5.4	5.1	1.5	-
128.838440	42.660007	0.091694	16.15	13.6	0.48	6.2	6.2	2.9	-
131.831635	3.341675	0.072952	16.12	13.4	0.65	4.6	4.6	4.5	-
135.309357	51.391785	0.129297	17.32	14.3	0.56	5.2	2.4	1.2	-
135.702240	54.159458	0.101710	16.37	13.6	1	3.8	3.5	2.9	-
135.886566	1.210117	0.058030	16.13	13.2	0.37	4.5	4.1	3.8	-
135.887466	1.208835	0.057939	17.33	13.2	0.37	4.5	2.2	1.8	-
135.991104	55.244137	0.089378	17.57	14.8	0.49	4.6	4.1	3.1	-
136.103760	53.937237	0.140552	17.61	14.7	0	6.1	5.7	3	-
136.583054	52.363892	0.098701	17.52	15	0.69	6.3	6.3	1.5	-
136.752792	0.060915	0.164117	17.26	14.2	0.85	4.9	4.8	4.6	3.6
138.115753	53.706375	0.222322	17.3	14.1	0.93	6.4	6.4	1.5	-
139.567947	56.832035	0.115982	16.61	13.7	0.53	4.3	2.9	1.5	-
141.083755	3.248529	0.129099	16.61	13.6	0.38	4.5	4.3	13.8	-1.4
144.678787	0.030188	0.090723	16.07	13.1	0.47	5	5	3.9	-
145.353928	57.963165	0.081976	16.44	13.7	0.94	4.2	4.3	1.8	-
147.077835	2.501155	0.060456	16.27	13.4	0.29	6.4	6	2.4	-
148.432892	-0.090180	0.083397	16.54	13.7	0.52	5.2	5	1.8	6.1
149.374603	2.828351	0.216094	17.33	14.4	0.78	5.5	5.4	0.8	-
153.439102	1.270462	0.105583	16.18	13	0.46	6.8	6.7	5.2	8.2
153.656876	1.157441	0.144184	16.8	13.9	0.84	4.3	4.4	0.3	-
153.832031	1.061565	0.215896	17.1	14.3	0.82	6	5.9	0.6	-
154.121719	-0.026977	0.104553	17.3	14.4	0	5.5	5.3	3.6	2.7
160.627304	0.578335	0.100022	16.63	13.9	0.7	6.7	6.7	4.2	-
168.387756	0.833713	0.152380	17.56	14.8	0.78	5	4.6	2.3	-
168.903183	-0.029248	0.143258	17.51	14.6	0.69	4.6	2.8	3.4	-
177.656357	1.500157	0.077820	16.4	13.6	0.74	6.6	6.8	2.9	-
181.079483	-0.315507	0.093782	15.18	12.6	0.38	7.4	7.1	1.9	-
183.690933	-0.919306	0.104813	17.18	14.1	0.16	4.8	4.3	5.7	9.4

continued on next page

Table 1 continued

RA	Dec	z	r'	K_s	B/T	$W_o(H\delta)$	$H\delta_A$	$W_o(O[II])$	$W_o(H\alpha)$
(J2000)			(mag)					(Å)	
185.485245	0.163395	0.106243	16.3	13.8	0.76	7.4	7.3	2.6	-
186.827286	-0.407924	0.114163	16.98	14.3	0.46	5.6	5.2	2.2	-
190.720642	2.616917	0.084382	17.52	14.9	0.4	6	6	2	1.4
192.314362	-0.630072	0.168910	17.49	14.2	0.17	5.5	3.6	2.5	8.8
195.686630	3.319118	0.068262	16.48	13.2	0.51	4.9	4.8	7.4	8.1
196.580307	-0.982160	0.246145	17.29	14.1	N/A	4.8	4.8	1.5	-
198.945999	-0.060723	0.197286	17.41	14.2	0.56	6.5	6.1	5.8	7.2
199.770584	0.519567	0.081329	17.56	14.8	0.9	5.6	5.5	5	1.6
205.427032	2.342579	0.075595	16.36	13.7	0.27	4.9	4.6	2.2	-
207.009094	2.068259	0.067782	15.91	13.3	0.67	6	6.1	2.1	-
207.554733	2.790413	0.106089	16.39	13.4	0.85	4.4	4.3	4.5	10
207.628204	1.467977	0.072761	15.9	13.4	0.64	6.6	6.6	3.2	1
209.131607	-0.268947	0.163201	17.26	14.4	0.55	4.2	4.4	3.9	1.1
213.135956	0.098394	0.126709	17.39	14.2	0.06	5.3	-1.3	-	4.2
214.725433	5.096523	0.079549	16.35	13	0.54	6.2	6.1	6.3	2.5
217.917770	3.031690	0.152753	17.66	14.7	0.52	4.4	4.2	1.1	-
218.522186	4.967597	0.087605	17.56	15	0.63	5.9	6.1	3.2	-
218.558441	3.027856	0.301874	17.71	14.7	0.44	5.8	5.3	1.4	1.6
218.704910	-0.155541	0.129915	17.66	14.6	0.56	6.4	-0.3	2.3	-
218.929077	0.948110	0.120438	17.27	14.5	0.9	6.1	5.4	3.8	1.2
219.054184	3.475608	0.119374	16.95	14	0.43	4.2	4.1	6.2	10.1
219.671616	0.173685	0.105131	17.14	14.4	0.78	4.9	4.6	4.1	-
221.547577	-0.238415	0.080029	17.33	17.8	0.03	5	4.3	3.7	9.5
222.647125	3.744416	0.116050	17.66	13.4	0.52	5.9	5.5	5.2	4.1
222.891068	2.449617	0.096892	17.16	14.5	0.59	4.7	4.8	1.8	-
223.189453	2.889261	0.264362	17.74	14.8	0.63	6.8	6.6	1.5	-
237.330612	57.389172	0.225225	17.35	14.4	0.72	5.3	4.9	0.4	-0.8
238.179855	54.813190	0.204227	17.65	14.5	0.44	5.1	1.6	0.4	-0.7
238.676956	54.844582	0.094013	17.62	14.7	N/A	5.4	2.2	8.4	1.1
239.025391	51.711884	0.123737	17.07	14.3	0.55	4.9	4.1	2.1	-1.3
240.205154	54.298256	0.064590	16.47	13.6	0.21	7.4	6.7	-	6.9
240.544449	2.751429	0.244081	17.36	14.5	0.45	6.2	6.2	1.9	-1.5
242.703766	50.720726	0.104457	16.77	14	0.8	5.6	5.5	2.9	1.1
246.983154	48.014202	0.125929	17.49	14.7	0.73	5.2	5.1	0.8	-
247.999588	43.298462	0.225063	17.67	14.5	0.75	4.6	3.5	1.2	-
249.646042	44.063736	0.112326	17.45	14.5	0.56	6.7	6.8	2.8	7.6
250.729843	41.893227	0.072600	16.15	13.4	0.64	6.5	6.7	1.2	-
251.366440	45.754738	0.154507	17.51	14.7	0.48	4.4	4.3	0.9	-1.2
252.795532	37.726040	0.136950	17.4	14.8	0.08	7.2	7.2	9.4	2.5
256.673676	38.576031	0.125296	17.45	14.6	0.71	5.5	5.3	6.5	1.9
258.942749	58.382076	0.127103	17.42	14.7	0.48	6.5	5.3	2.2	1.3
262.832245	55.128433	0.102557	16.95	14.3	0.64	5.7	5	5.2	-
263.207581	54.367542	0.161453	17.37	14.8	0.64	7	6.7	4.9	7.3
265.387665	54.057060	0.113601	17.41	14.7	0.79	5.7	6.2	3.7	-
309.355164	-6.660254	0.114976	17.15	14.1	0.72	4.5	4.1	2.3	-
310.385773	-5.226147	0.062059	16.73	14.1	0.62	5.3	4.8	2.9	1.9
315.745331	10.550177	0.092800	15.22	12.5	0.58	4.7	4.4	1.3	-
318.271515	-7.736905	0.088147	17.62	14.9	0.59	6.1	5.6	5.2	-
320.108154	-6.913008	0.224315	17.42	14.6	0.63	5.2	5	9	5.1
320.151672	-6.622945	0.119113	17.54	14.8	0.76	5	4.1	2.7	-
326.767517	10.954961	0.083870	16.53	13.9	0.35	4.4	4.2	4.3	-
327.472046	0.969026	0.172979	17.47	14.3	0.55	5.5	2.6	13.9	-0.4
327.512482	-7.130242	0.083176	17.53	14.8	0.22	6.1	4.1	4	9.4
327.862793	12.987449	0.206182	17.36	14.6	0.46	6.6	6.5	9.9	2.3
328.255249	-7.838636	0.073321	17.26	14.2	0.38	5.3	1.6	3.7	-
328.746399	-6.853999	0.216543	17.09	14.1	0.7	6.3	5.9	2.4	-
329.933380	12.793406	0.122527	16.47	13.6	0.56	5.8	5.7	5.7	5.8
331.439728	-9.487941	0.135392	17.71	15	0.43	6	5.9	3.2	-

continued on next page

Table 1 continued

RA (J2000)	Dec	z	r' (mag)	K_s	B/T	$W_o(H\delta)$	$H\delta_A$	$W_o(O[II])$ (Å)	$W_o(H\alpha)$
340.961884	-10.229675	0.085119	17.63	14.9	0.29	5.1	4.7	8.2	1.2
341.995117	-9.762263	0.177042	17.69	14.6	0.61	5	0.8	-6.2	0
344.118774	14.673409	0.163308	17.09	14.2	0.64	5.1	4.6	6.3	-
344.236511	13.067387	0.209131	17.18	14.4	0.72	6.7	6.6	2.4	-
345.029846	15.317498	0.082219	16.89	14	0.56	6.1	5.8	3.8	1.7
345.367645	-8.565503	0.181151	17.36	14.4	0.53	5.1	4.9	3	0.9
346.157288	14.149549	0.122222	16.53	13.7	0.48	4.6	4.4	3.8	2.6
346.930847	15.432889	0.069696	16.17	13.8	0.45	6.3	6.3	1.7	-
348.280731	15.481363	0.109839	17.03	13.8	0.44	5	5.1	7.2	7.1
349.948700	0.721130	0.118550	17.28	14.5	0.72	5	4.4	3.8	-
353.721649	14.846871	0.064671	15.98	13.4	0.56	4.9	4.5	1.6	-
355.495483	14.908378	0.085547	16.73	13.9	0.6	5.5	5.9	6.6	2.6
358.630005	14.332058	0.078535	15.69	12.9	1	3.9	4	4.4	1.4

Column descriptions: (1-2) Right ascension and declination; (3) Redshift; (4) SDSS r magnitude; (5) K_s magnitude measured from our UKIRT data. Uncertainties are limited by the zeropoint and are ~ 0.08 magnitude; (6) The fraction of K-luminosity in the bulge component, and uncertainty, as determined by GIM2D model fits. Note that these are meaningless in irregular systems (such as close pairs or mergers); (7) rest-frame equivalent width of $H\delta$, in Å, from Goto et al. (2003), where positive numbers represent absorption; (8) rest-frame equivalent width of $H\delta$ based on the definition of Worthey & Ottaviani (1997); (9-10) Rest-frame equivalent widths of [OII] and $H\alpha$ from the SDSS pipeline, measured in Å with positive numbers indicating emission.

Table 2: The e(a) galaxy sample and measured properties

RA (J2000)	Dec	z	r' (mag)	K_s	B/T	$W_o(H\delta)$	$H\delta_A$	$W_o(O[II])$ (Å)	$W_o(H\alpha)$
0.304384	-11.103624	0.119084	16.44	13.4	0.31	5	4.8	19.9	47.3
1.336491	-10.469523	0.076842	16.7	14.1	0.01	7.2	4.8	-	40.6
2.689777	-0.127752	0.086695	16.53	13.7	0.09	5.3	5.1	13.5	32.8
4.726562	-11.208706	0.060786	16	13.8	0.49	7.1	4.7	29.9	51.7
5.937845	-1.008309	0.066280	17.14	13.9	0.33	5.7	5.3	10.2	14.4
7.592993	15.013621	0.098497	16.15	13.4	0.08	6	4.6	10.3	31.6
10.653961	-1.029383	0.252882	18.52	15.4	0.57	5.4	2.9	16.4	37.8
10.851816	0.016397	0.081329	16.09	13.5	0.12	7	4.1	19.5	67.5
14.807940	0.794905	0.172719	18.02	15.1	0.23	5.9	4	29.7	47.9
15.323996	0.524027	0.145131	17.49	14.6	0.2	6.2	4.6	11.6	35.6
16.047445	-10.786201	0.082317	17.68	15	0.44	6.1	5.9	25.5	15.3
16.591736	-0.535420	0.171226	17.3	14	0.61	4.6	4.4	30.7	34.9
17.969322	-9.766603	0.131466	17.35	13.9	0.61	5.1	5.1	35.5	31.7
21.064075	14.038528	0.103083	17.4	13.9	0.15	5.9	3.5	4.3	20.8
21.218010	-9.570095	0.074324	16.78	13.6	0.79	5.2	5.3	18.8	8.1
24.083879	14.578506	0.107873	17.41	14.6	0.16	5.1	4.6	9.5	37
24.298273	13.111508	0.054026	16.28	13.8	0.12	5.4	5	22.1	28.8
24.492804	-8.575119	0.189068	17.39	13.5	0.88	4.7	4.6	15.3	32.2
27.441174	0.808579	0.162652	17.31	14.3	0.29	5	4.9	8.3	25.6
29.266397	13.594388	0.100934	16.43	13.5	0.64	4.5	4.5	-	34.6
29.476841	14.095569	0.178564	17.49	14.5	0	5.1	4.5	8.8	37.5
35.197891	-9.624654	0.108725	16.85	13.6	0.57	4.7	4.5	17.3	17.6
40.521065	-8.866433	0.110401	16.04	13.1	0.24	4.5	4.3	8.9	34.9
41.083641	-7.754149	0.076250	15.55	12.9	0.71	4.6	4.7	22.2	39.2
46.296959	-6.431061	0.086905	17.53	15.3	0	5.9	6	10.9	15.9
52.038315	-7.305844	0.086911	17.64	15.2	0.05	5.2	5.2	-	32.7
62.729263	-6.176466	0.129256	17.35	14.1	0.34	5.5	4.6	19.3	34
116.479462	32.579166	0.100922	17.21	14.3	0.06	5	5	6.5	16.3
117.033798	42.903248	0.113352	17.66	14.6	0.28	5.4	4	8.1	21
119.685112	40.516521	0.074947	16.72	13.8	0.44	5.5	4.7	4	16.5
123.469513	40.901772	0.100391	17.33	14.1	0.07	5	2.6	5.4	12.6
130.364212	3.535027	0.143611	17.44	14.4	0.67	4.7	4.5	2.9	13.6
133.691208	48.470387	0.119963	17.41	14.2	0.03	4.7	2.3	4.6	19.1

continued on next page

Table 2 continued

RA (J2000)	Dec	z	r' (mag)	K_s	B/T	$W_o(H\delta)$	$H\delta_A$	$W_o(O[II])$ (Å)	$W_o(H\alpha)$
148.434738	−0.090464	0.083706	15.64	13.7	0.52	5.2	3	13.3	33.3
148.655762	2.207545	0.162581	17.25	14.1	0.76	5.4	4.1	6	19
163.710587	−0.982576	0.074838	17.55	14.8	0.23	5.2	4.8	7.2	16.3
166.723526	1.249782	0.105472	16.09	12.9	0.36	4.6	4.1	4.9	14.8
173.176758	0.756327	0.067486	16.83	12.8	0.71	5.5	6.1	19.7	26
175.077286	1.076113	0.076980	16.6	13	0.71	10.5	8.3	9.7	19.7
189.067123	−0.386185	0.090503	17.29	14.6	0.86	5.6	5.9	11.6	1.8
197.523224	−2.472836	0.132543	17.52	14.6	0.13	4.6	4.8	10.4	12.1
198.926941	−1.724550	0.175708	17.48	14.3	0.04	6.8	2.4	5.1	18.4
201.826462	0.865157	0.111664	17.18	14.3	0.31	5.3	4.3	5.4	18.7
210.408279	0.067353	0.085131	15.66	13.1	0.18	4.3	4	5.8	15
214.608963	1.356086	0.083081	16.46	13.6	0.28	5.2	4	3.3	16.8
222.645447	3.745237	0.115040	16.8	13.4	0.52	5.9	0.1	42.8	78.8
239.997879	54.588268	0.057877	16.63	13.7	0.01	5.7	3.1	5.4	20.4
240.273132	49.979671	0.071001	15.43	12.6	0.25	6	5.6	30.7	34.4
241.539871	51.154034	0.077398	17.19	14	0	7.4	2.6	8.5	18.6
246.701721	45.584122	0.086421	17.24	14.3	0.13	7.6	5	13.6	28.5
247.959869	44.898746	0.222740	17.28	14.3	0.3	4.2	4	28.6	37.3
248.377213	43.259373	0.122890	16.73	14.4	0.21	7.2	5	26.4	58.3
252.343353	38.528667	0.086168	16.32	13.9	0.05	5.9	4.7	19.2	41
253.869644	40.062359	0.061714	16.98	14.7	0	4.9	4.8	33.2	46.9
254.030594	38.869167	0.073432	17.17	13.9	0.01	6.6	5	13.5	26.3
254.062775	38.859486	0.051833	15.95	12.6	0.47	5.1	4.8	15.4	27.6
258.726166	55.708164	0.106540	16.74	13.7	0.68	6.2	4.8	10.4	25.3
260.090363	54.825855	0.100796	17.57	14.3	0.58	6	4.1	8	20.5
260.632111	52.869144	0.159600	17.03	14.2	0.36	6.2	4.3	14.6	38.3
262.566376	54.298878	0.085144	16.93	14.2	0.2	4.6	4.3	4.7	16.8
264.509949	55.871490	0.084523	16.73	13.8	0.12	5.7	4.3	15.3	31.3
309.668823	−4.640462	0.229230	17.3	14.1	0.1	6.6	4.8	5	23.6
309.947723	−6.421526	0.111621	17.36	14.7	0.18	5	4.5	25.6	39.3
316.396729	−6.442801	0.086264	17.2	13.8	0.28	5.8	5.2	15.7	15
317.146118	−8.015185	0.122152	16.71	13.2	0.52	4.8	5	4.1	14.7
318.084625	−7.201864	0.098725	16.63	13.2	0.39	6	5.6	4508.6	2.7
322.490906	−8.057539	0.219952	17.25	14.4	0.69	4.3	4.3	4.7	24.5
322.521881	−6.686210	0.089172	14.52	15.2	0.32	5	3.6	91.5	38.4
323.297852	−8.495975	0.091285	17.29	14.3	0.5	5.2	3.3	7.8	15.5
323.427399	−8.360456	0.117046	16.4	13.4	0.64	6.7	5.7	10.8	28.4
327.134552	0.133313	0.158565	17.64	14.5	0.46	5.4	4.6	7.1	14
327.349152	−8.675175	0.102440	17.14	13.7	0.93	5	3.8	17	30.6
327.423340	12.339659	0.076621	16.81	13.9	0.28	4.8	5	5.4	15.5
327.666290	−1.073946	0.103408	17.23	14.7	0.26	5.3	4.9	19.1	29.9
327.735779	−6.819699	0.058740	15.98	13.3	0.8	4.7	5.2	24.6	13.9
327.868164	−6.775196	0.101240	16.67	13.9	0.95	7.4	6.9	16	19.6
330.465393	12.099227	0.123104	16.06	13.1	0.55	5.8	5.5	26.1	35
330.580353	−0.565185	0.084469	17.62	12.9	0.09	7	7.2	14.4	24.1
334.127258	−0.574393	0.111474	16.73	14	0.87	6.4	4.7	25.1	38.9
334.428925	−0.290766	0.094682	16.96	14.1	0.36	5.6	4.6	25.8	47.4
334.805664	12.976340	0.106792	17.31	14.4	0.4	5.1	4.8	20	44.3
336.138947	0.579151	0.090261	18.97	16.6	0.08	5.7	5.5	16	29.1
340.294891	−9.014417	0.071547	15.59	12.3	0.22	5.4	4.6	15.4	34.9
340.507233	−8.774342	0.166393	17.76	13.6	0.28	5.6	5.3	15.4	11.7
340.507812	−8.773771	0.166596	17.64	13.6	0.28	5.6	5.4	11.6	4.9
342.494751	0.918355	0.089213	16.47	13.9	0.06	5.1	5.3	15.3	35.4
342.842072	−8.956442	0.080072	17.22	14.4	0.54	5.8	5.9	33.6	21.9
346.197815	14.275584	0.082477	17.02	14.7	0.11	7.5	7.2	22.5	28.9
346.333771	−9.530315	0.183999	17.38	14.2	0.55	5.4	5.5	4.4	12.3
346.764313	−10.351763	0.104952	17.13	14.2	0.12	4.9	5	14	16.1
348.372345	0.909661	0.120993	17.36	14.3	0.22	6.9	2.1	8.1	12.1

continued on next page

Table 2 continued

RA	Dec	z	r'	K_s	B/T	$W_o(H\delta)$	$H\delta_A$	$W_o(O[II])$	$W_o(H\alpha)$
(J2000)			(mag)					(\AA)	
356.560333	13.656058	0.077711	17.1	14.2	0.12	6.5	4.6	9.9	26.7
358.733002	-10.032640	0.111582	17.27	14.3	0.64	5.6	4.6	33.5	84.8
358.946411	16.096483	0.102185	17.66	14.3	0.18	6.2	5.7	10.8	18.3

APPENDIX A: GALAXY MORPHOLOGIES

In this appendix we present images for a subset of our sample. Figures A1–A3 show all of the k+a galaxies, sorted by B/T ratio. Figures A4–A5 show the same for a representative sample of k+a–like galaxies with weak emission lines ($W_o(H\alpha) < 10\text{\AA}$ and $W_o([OII]) < 10\text{\AA}$). There are another nine of these galaxies in our sample, not shown here: all but one have $B/T > 0.5$. Finally, in Figures A6–A8 we show images for 60 of the 94 e(a) galaxies; Figure A6 shows the twelve bluest e(a) galaxies, while Figures A7 and A8 show a representative subsample of the remaining e(a) galaxies with disk–dominated morphologies or bulge–dominated morphologies, respectively. In each panel we label the B/T measurement and the galaxy ID number. A star is shown in the upper–left corner of the image if we have identified it as possibly interacting.

Figure A1. K – band images and model fits for k+a galaxies with $B/T \leq 0.52$. In each set of three images, the left image is the central $12''$ of the original image; the middle panel shows the GIM2D model fit; and the right panel shows the residual between the model and the data. Contours shown on the model fits are logarithmically spaced. The B/T value and galaxy id are given above each set of three images. A star is shown in the upper-left corner of the image if we have identified it as possibly interacting; note that this identification is often based on features that are either difficult to discern on these small images, or are outside the image boundaries.

Figure A2. As Figure A1, but for k+a galaxies with $0.52 < B/T < 0.7$.

Figure A3. As Figure A1, but for k+a galaxies with $B/T \geq 0.7$.

Figure A4. As Figure A1, but for a representative subsample of k+a galaxies with a small amount of emission ($W_o(\text{H}\alpha) < 10\text{\AA}$ and $W_o([\text{OII}]) < 10\text{\AA}$) and $B/T < 0.5$. There is one other galaxy in our sample satisfying these criteria, but not shown.

Figure A5. As Figure A4, but for $B/T > 0.5$. There are an additional 8 galaxies in this category, not shown here.

Figure A6. As Figure A1, but for the bluest e(a) galaxies, with $(u - g) < 1.1$ and $(r - k) < 2.7$.

Figure A7. As Figure A1, but for a representative sample e(a) galaxies with $B/T < 0.5$, excluding those shown in Figure A6. There are another 31 galaxies of this type not shown.

Figure A8. As Figure A7, but for $B/T > 0.5$, and excluding those shown in Figure A6. There are another 3 galaxies of this type, not shown.

This figure "FigA1.gif" is available in "gif" format from:

<http://arXiv.org/ps/astro-ph/0503639v1>

This figure "FigA2.gif" is available in "gif" format from:

<http://arXiv.org/ps/astro-ph/0503639v1>

This figure "FigA3.gif" is available in "gif" format from:

<http://arXiv.org/ps/astro-ph/0503639v1>

This figure "FigA4.gif" is available in "gif" format from:

<http://arXiv.org/ps/astro-ph/0503639v1>

This figure "FigA5.gif" is available in "gif" format from:

<http://arXiv.org/ps/astro-ph/0503639v1>

This figure "FigA6.gif" is available in "gif" format from:

<http://arXiv.org/ps/astro-ph/0503639v1>

This figure "FigA7.gif" is available in "gif" format from:

<http://arXiv.org/ps/astro-ph/0503639v1>

This figure "FigA8.gif" is available in "gif" format from:

<http://arXiv.org/ps/astro-ph/0503639v1>